



**HAL**  
open science

## Optical diffraction of fractal figures: random Sierpinski carpets

Denise Berger, Stéphane Chamaly, Michel Perreau, Daniel Mercier, Pascal Monceau, Jean-Claude Serge Levy

► **To cite this version:**

Denise Berger, Stéphane Chamaly, Michel Perreau, Daniel Mercier, Pascal Monceau, et al.. Optical diffraction of fractal figures: random Sierpinski carpets. *Journal de Physique I*, 1991, 1 (10), pp.1433-1450. 10.1051/jp1:1991217 . jpa-00246426

**HAL Id: jpa-00246426**

**<https://hal.science/jpa-00246426>**

Submitted on 4 Feb 2008

**HAL** is a multi-disciplinary open access archive for the deposit and dissemination of scientific research documents, whether they are published or not. The documents may come from teaching and research institutions in France or abroad, or from public or private research centers.

L'archive ouverte pluridisciplinaire **HAL**, est destinée au dépôt et à la diffusion de documents scientifiques de niveau recherche, publiés ou non, émanant des établissements d'enseignement et de recherche français ou étrangers, des laboratoires publics ou privés.

Classification

Physics Abstracts

61.10D — 61.90 — 42.30

## Optical diffraction of fractal figures : random Sierpinski carpets

Denise Berger <sup>(1)</sup>, Stéphane Chamaly <sup>(1)</sup>, Michel Perreau <sup>(2)</sup>, Daniel Mercier <sup>(2)</sup>, Pascal Monceau <sup>(2)</sup> and Jean-Claude Serge Levy <sup>(2)</sup>

<sup>(1)</sup> Laboratoire d'Optique Physique (\*), E.S.P.C.I., 10 rue Vauquelin, 75231 Paris Cedex 05, France

<sup>(2)</sup> Laboratoire de Magnétisme des Surfaces, Université Paris 7, 75251 Paris Cedex 05, France

(Received 25 January 1990, revised 3 June 1991, accepted 24 June 1991)

**Résumé.** — On présente ici les clichés de diffraction optique de tapis de Sierpinski aléatoires de différentes dimensions fractales, pris à des niveaux d'itération différents. Au moyen du formalisme de la matrice de transfert dans les fractals, on montre la sensibilité de cette analyse expérimentale aux corrélations à moyenne et longue portée. Ainsi la relation entre les sous-dimensions fractales du F.M.T. et les rapports d'intensité entre les clichés de diffraction de figures fractales à des niveaux d'itération différents est soulignée. Enfin on esquisse le principe d'une analyse expérimentale de ces nouvelles dimensions théoriques.

**Abstract.** — The optical diffraction patterns of random Sierpinski carpets of different fractal dimensions at different levels of iteration are shown and analyzed. The sensitivity of such an analysis to long range correlations, is demonstrated theoretically by means of the transfer matrix formalism of fractals, T.M.F. The relation between the subdimensions defined in T.M.F. and diffraction patterns is outlined. Finally an analysis of experimental diffraction patterns is proposed in order to measure these new theoretical subdimensions.

### Introduction.

The optical diffraction of bidimensional structures is well known to be a powerful tool for investigating the short and long range order in 2d structures [1, 2]. This tool has become more and more practical since convenient coherent sources such as lasers became available. For instance, numerous optical diffraction patterns were obtained for structures with fivefold symmetry : Penrose's tilings [3, 4], Robinson's tilings [5]. They have been compared to the diffraction patterns obtained from an electron beam or an X ray beam on quasicrystalline materials of the icosahedral I phase [6] or of the decagonal T phase [7], with the evidence of a two-dimensional phase with fivefold symmetry as the T phase. Recently Allain and Cloitre [8] computed the diffraction patterns of a deterministic Koch set. Here we chose to investigate a rather large class of fractals : the random Sierpinski carpets  $C(n, p)$  where the iteration process consists in a segmentation of each square into  $n \times n$  subsquares conserving among

(\*) ER5 du CNRS.

them only  $p (\leq n^2)$  subsquares at the next step of iteration. These  $p$  subsquares are chosen at random. The fractal dimension  $d_f: \text{Ln}(p)/\text{Ln}(n)$  can be considerably varied, and the randomness introduced in the choice of subsquares strongly enhances the number of relevant configurations at the expense of inherent fluctuations. These RSC are good examples of fractal structures [9] and there is abundant literature about phase transitions on them. Moreover, numerous analytical properties of the structure of these random Sierpinski carpets have already been obtained [10], and these properties reveal themselves useful to understand the diffraction patterns. Among these properties, percolation, i.e. the appearance of an infinitely connected cluster, is known to occur for structures with fractal dimension lower than 2 [9]. Thus a threshold of percolation must be observed when considering a series of random Sierpinski carpets which covers a large range of fractal dimensions. Since percolation is, by definition, a long range property, the optical diffraction which is sensitive to long range effects, must be sensitive to percolation. This defines the first aim of this work, which is to see if and how optical diffraction can be sensitive to percolation and how diffraction is sensitive to a fractal structure. Secondly, Mandelbrot *et al.* [11] developed a transfer matrix formalism, T.M.F. for the analysis of border properties in deterministic and random Sierpinski carpets, what led two of us (M. Perreau and J. C. S. Lévy) to generalize the TMF in order to study the evolution of local connectivity in random Sierpinski carpets [10]. In the Sierpinski  $C(n, p)$ , the six different states of local connectivity of a square are: isolated, with one occupied neighbor, with two occupied neighbors which are opposite or not, with three occupied neighbors and with four occupied neighbors, as shown in figure 1. The analysis of the evolution of these states of local connectivity during iteration by means of transfer matrix defines eigenvalues and thus subdimensions which are useful to describe the probability of a state of connectivity at a given step. This defines an internal structuration of the fractal  $C(n, p)$  which is expected to be observed by diffraction methods. This is the second aim of this paper. Since the result of the analysis of the connectivity is the evidence of a lower threshold for percolation in  $C(n, p)$  with  $d_f = 3/2$  [10, 12], it defines a third aim to this paper namely what happens to diffraction patterns for  $C(n, p)$  with  $d_f$  close to  $3/2$ .

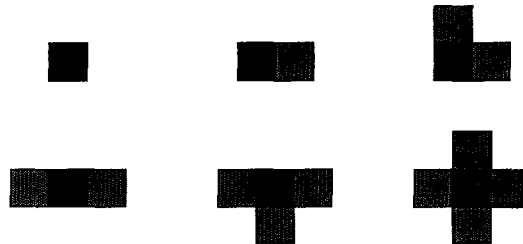


Fig. 1. — The six states of local connectivity of a unit square in a Sierpinski carpet.

Practically a large variation of diffraction patterns for different  $p$  is observed in agreement with theoretical arguments but the inherent fluctuations of  $C(n, p)$  are rather strong and make the estimations of the subdimensions difficult, even if self-similarity is well observed.

The experimental preparation of optical targets and optical diffraction is described in section 1, while section 2 deals with theoretical predictions. In section 3 the diffraction patterns are shown and compared to predictions.

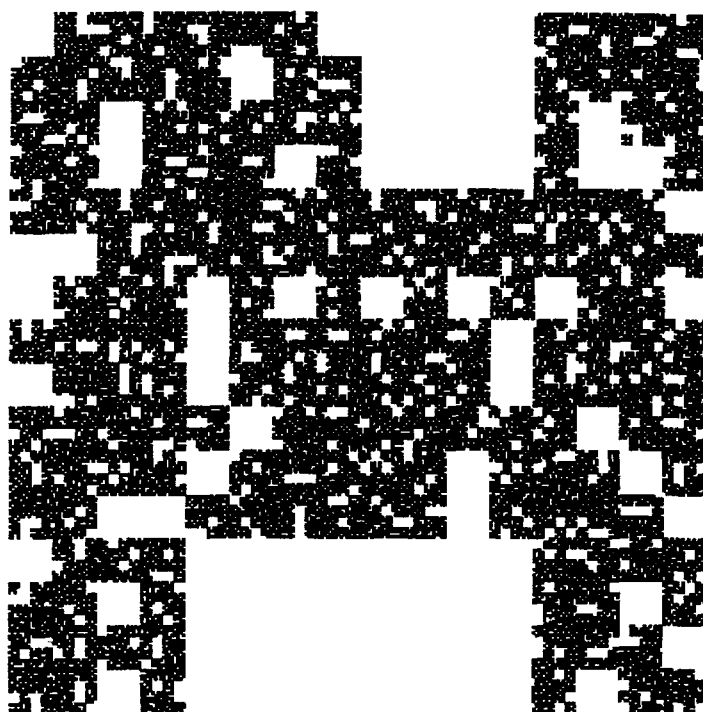
## 1. Experimental process.

### 1.1 GENERATION OF SETS OF SQUARES. —

Forgetting the inflation process in the definition of random Sierpinski carpets, instead of a plane tiling, a decoration of the unit square is obtained



a)



b)

Fig. 2. — Two sets of Sierpinski diffracting pupils, with four steps of iteration :  $C(4, p)$  with a)  $p = 7$ , b)  $p = 13$ . The case a is typical of a localized dust while the case b exhibits percolation from one edge to the opposite one.

for each  $C(n, p)$ . For a given  $n$ , there are  $n^2 - n - 1$  choices of  $p$  which define a fractal dimension of  $C(n, p)$  in the range 1 to 2. Thus, the practical choice of  $n = 4$ , gives 11 such cases with  $d_f(p)$ :

$p$	5	6	7	8	9	10	11	12	13	14	15	16
$d_f$	1.161	1.292	1.404	1.5	1.585	1.661	1.730	1.792	1.850	1.904	1.953	2

This rather regular sampling of fractal dimensionalities can approach each value within 0.06, which is correct for a first inspection. In a unit square of 6 inches by 6 inches, the result of 4 steps of iteration is plotted down, i.e. the  $p^4$  retained small squares are drawn in full black as shown in figure 2. There are  $4^8 = 65\,536$  such possible small squares. A photograph reduces the size of this unit square up to the admitted size of a laser spot expanded by means of usual optical means, while the reduced size of a small square remains large in front of the size of grains in the photographic emulsion, in order to avoid any confusion between grain and square effects.

**1.2 OPTICAL DIFFRACTION.** — Fourier transforms of the random Sierpinski carpets produced after 4 steps of iteration are obtained by classical Fraunhofer diffraction [1]. The sets of squares as shown in figure 2 are photographed on high contrast CBS4 Dupont film. And these films are lightened by the coherent spatially filtered beam of an He-Ne laser. The schema of the experiment is given in figure 3. The image of the diffraction pattern (FT) is projected onto a white screen (S) and then photographed. In order to avoid diffusion effects, direct laser light is eliminated by making an aperture in the screen.

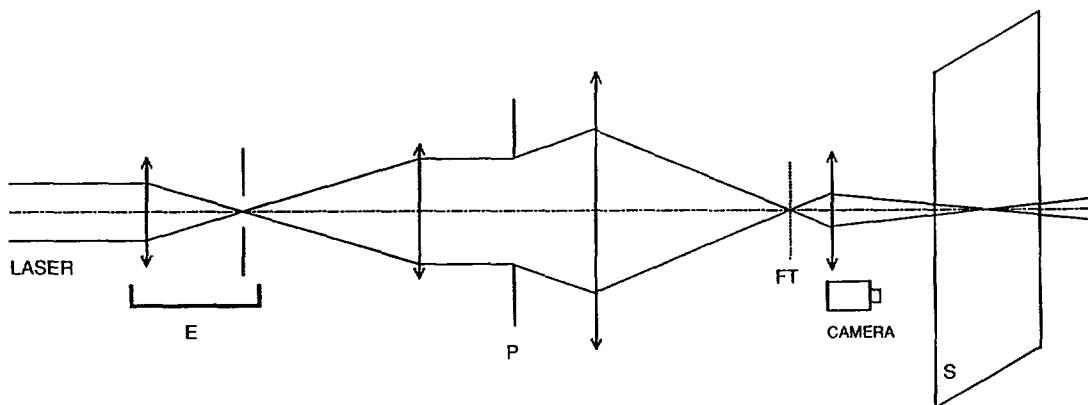


Fig. 3. — Schema of the experiment of optical diffraction.

Some diffraction patterns obtained for random Sierpinski carpets as shown in figure 2 are shown in figure 4.

## 2. Theoretical predictions.

In the plane of the slide, there are two axes  $Ox$  and  $Oy$  parallel to the sides of the squares, while the incident laser beam of wavelength  $\lambda$  has,  $\mathbf{u}_0$  for unit vector parallel to its propagation direction and normal to the slide. The unit vector  $\mathbf{u}$  parallel to the propagation direction of the diffracted beam makes an angle  $\theta$  with  $\mathbf{u}_0$ , and  $\theta$  is weak in front of 1 rad ( $\theta < 10^\circ$ ) because of experimental geometry. Thus the amplitude  $A_u$  of the resulting plane

wave which is diffracted by the running subsquare located at  $M$  and of weight  $\rho(M) dx dy$  is :

$$A_u = \iint \exp[2 i \pi \mathbf{u} \cdot \mathbf{OM} / \lambda] \rho(M) dx dy . \tag{1}$$

This formula and the fractal character of the figure, i.e. of  $\rho(M)$  lead to the diffraction pattern. But two quite different approximate approaches can be used : either one can use the symmetry of the square in order to factorize  $\rho(M)$  as  $\rho_1(x) \rho_2(y)$ , with (because of the symmetry between  $x$  and  $y$  axes)  $\rho_1(x) = \rho_2(x) = u(x)$ , or (because of the overall isotropy of the fractal) one can use  $dx dy \rho(M) = v(r) 2 \pi r dr$ . Both approaches are interesting as will be seen later since, according to the observation, either the global axis of symmetry or the local isotropy must be emphasized.

The first approach for a square  $S$  of side  $a$  gives :

$$\iint_S \rho(M) dx dy = \left[ \int_0^a u(x) dx \right]^2 = C a^{d_f} \tag{2}$$

and by differentiation :

$$u(x) = C^{1/2} (d_f/2) x^{\frac{d_f}{2}-1} \tag{3}$$

When  $\mathbf{u}$  is perpendicular to  $Oy$ , as achieved in the experimental measurement of the photomultiplier photocurrent, the diffraction amplitude reads :

$$A_u = \int_0^a \int_0^a \exp[2 i \pi \theta x / \lambda] C (d_f/2)^2 (xy)^{\frac{d_f}{2}-1} dx dy . \tag{4}$$

After integration over  $y$ , it reads :

$$A_u = C (d_f/2) a^{\frac{d_f}{2}} \int_0^a \exp[2 i \pi \theta x / \lambda] x^{\frac{d_f}{2}-1} dx \tag{5}$$

or :

$$A_u = C (d_f/2) \left( \frac{i \lambda a}{2 \pi \theta} \right)^{\frac{d_f}{2}} \int_0^{-\frac{2 i \pi \theta a}{\lambda}} e^{-v} v^{\frac{d_f}{2}-1} dv \tag{6}$$

after a change in the integration variable. The regularity of the integrand in the IVth quadrant if  $d_f > 0$ , and the large value of the upper bound ( $\theta a / \lambda$  is of order  $10^2$ ) enable us to write :

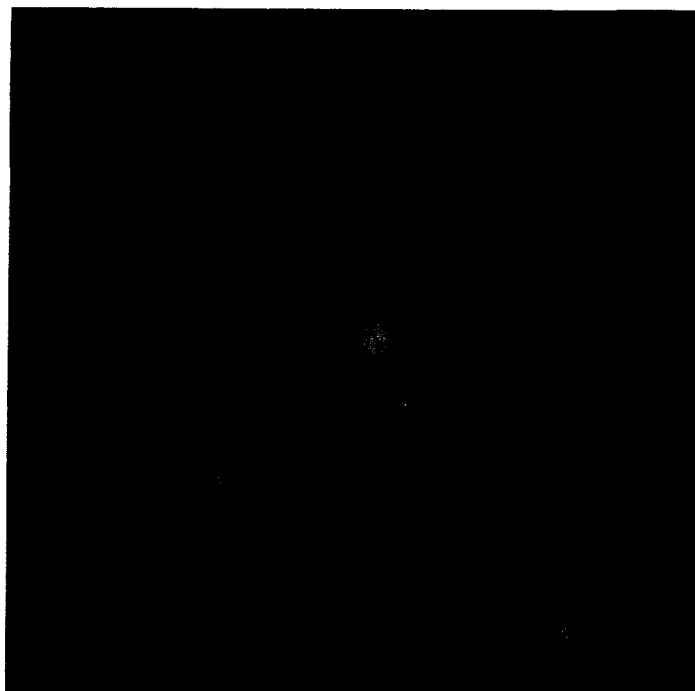
$$A_u = C \left( \frac{d_f}{2} \right) \left( \frac{i \lambda a}{2 \pi \theta} \right)^{\frac{d_f}{2}} \Gamma \left( \frac{d_f}{2} \right) \tag{7}$$

with the usual gamma function [13]. Thus the expected intensity  $I_u$  decreases with  $\theta$  as  $\theta^{-d_f}$ . In the second approach :

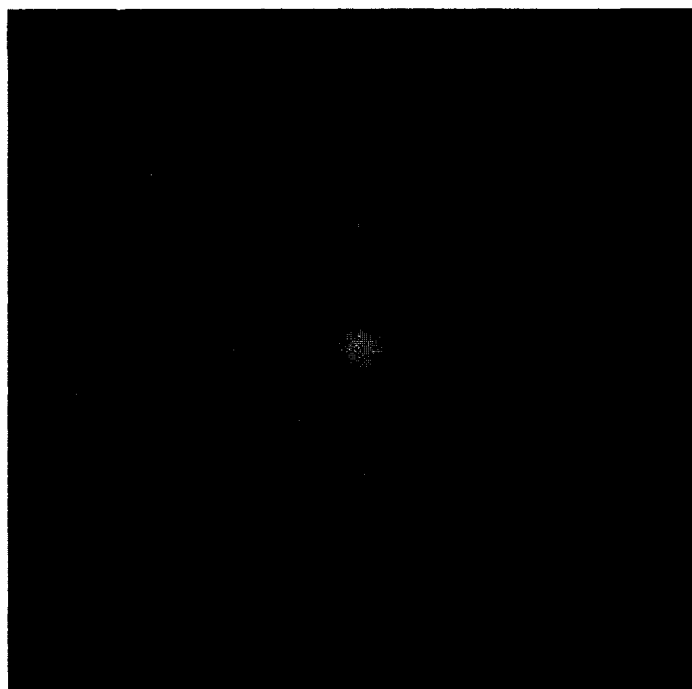
$$2 \pi \int_0^{a/2} v(r) r dr = D \left( \frac{a}{2} \right)^{d_f} \tag{8}$$

leads to

$$v(r) = (D/2 \pi) d_f r^{d_f-2} \tag{9}$$

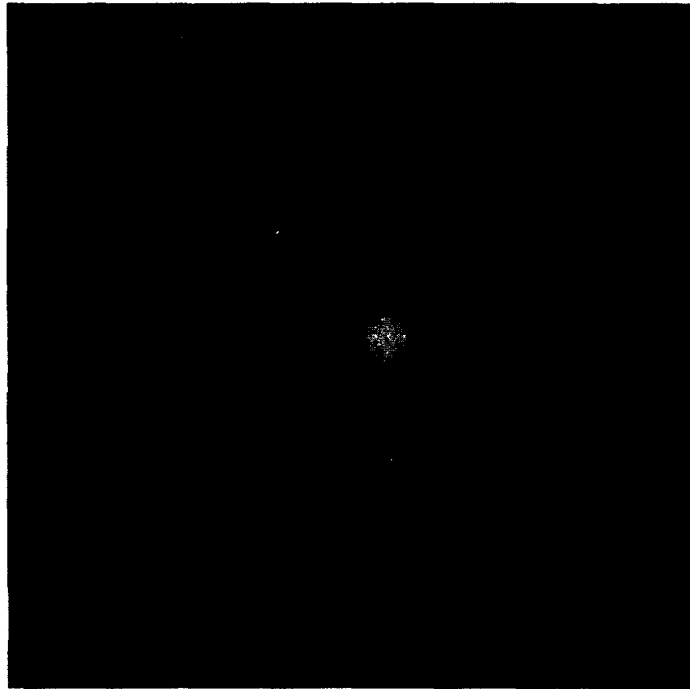


a)

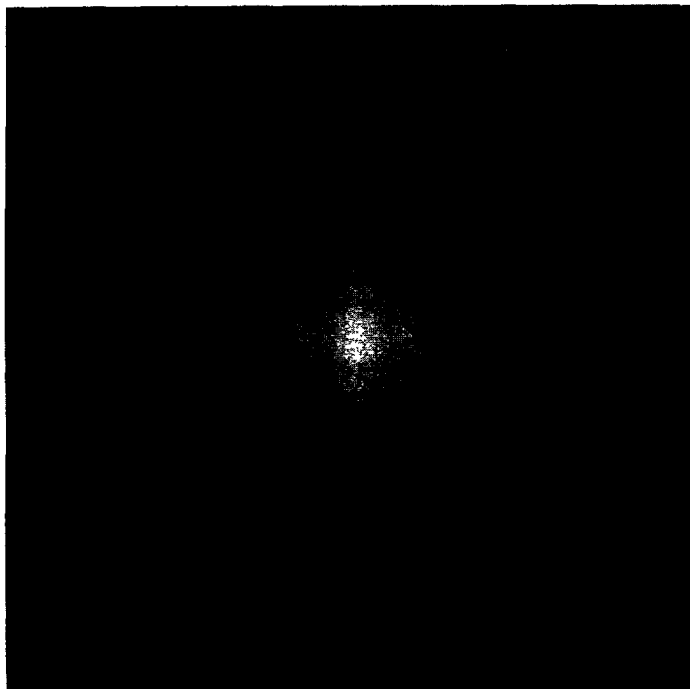


b)

Fig. 4. — Diffraction patterns obtained from pupils such as shown in figure 2. a)  $p = 6$ , b)  $p = 8$ , c)  $p = 9$ , d)  $p = 10$ , e)  $p = 11$ , f)  $p = 13$ , g)  $p = 14$ , h)  $p = 15$ .

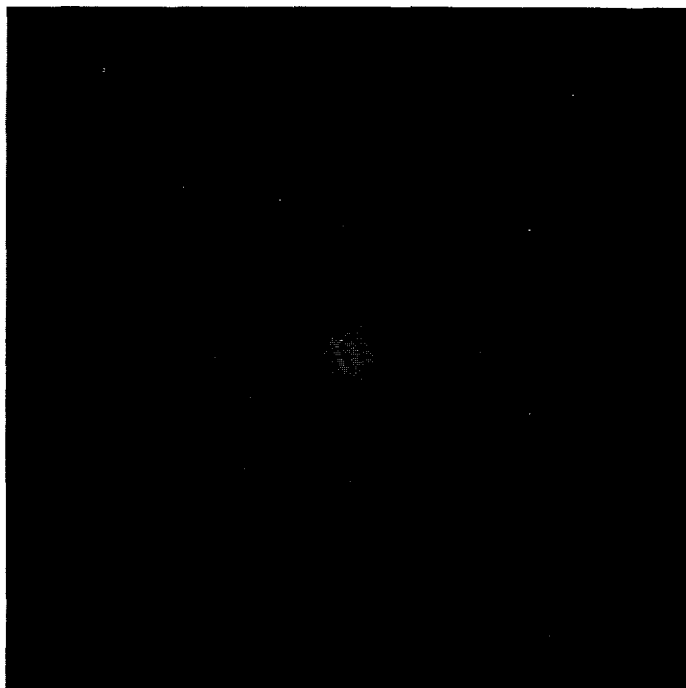


c)



d)

Fig. 4 (continued).

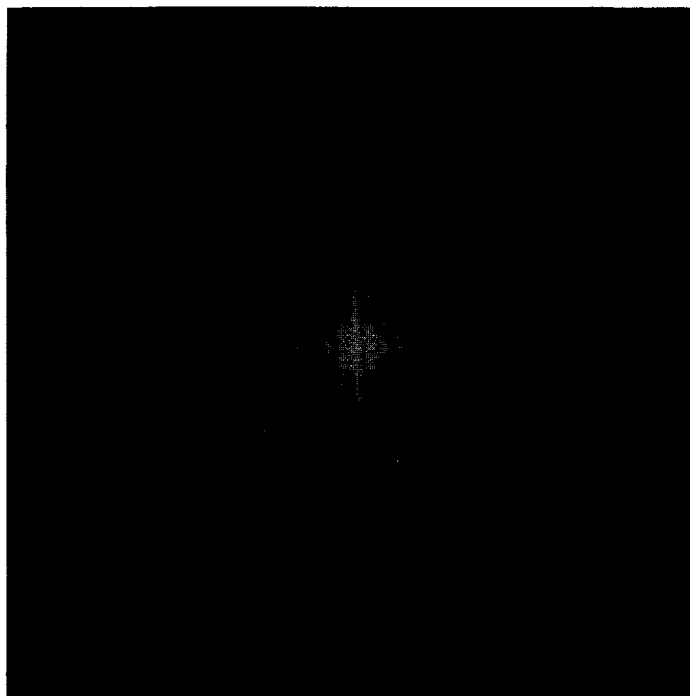


e)

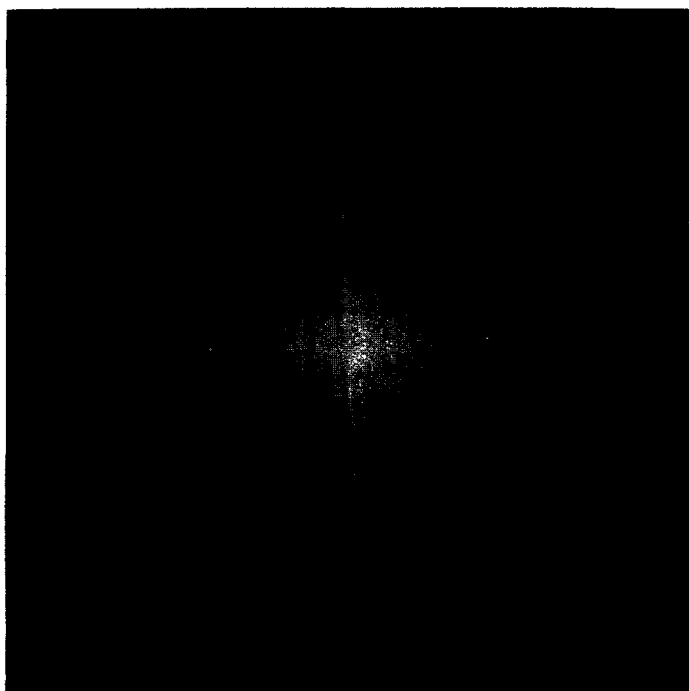


f)

Fig. 4 (continued).



g)



h)

Fig. 4 (continued).

The amplitude  $A_u$  in the same direction normal to Oy as before in equations (4, 5 and 6) reads :

$$A_u = \int_0^{2\pi} \int_0^{a/2} \exp[2i\pi\theta r \cos \phi/\lambda] (D/2\pi) d_f r^{d_f-1} dr d\phi \quad (10)$$

and integration over  $\phi$  [13] gives :

$$A_u = D d_f \int_0^{a/2} J_0\left(\frac{2\pi r\theta}{\lambda}\right) r^{d_f-1} dr = D d_f \left(\frac{\lambda}{2\pi\theta}\right)^{d_f} \int_0^{\frac{\pi a\theta}{\lambda}} J_0(t) t^{d_f-1} dt. \quad (11)$$

As noticed before in the first approach  $a\theta/\lambda$  is large and the asymptotic behaviour of the integral  $I(b)$  must be followed with interest :

$$I(b) = \int_0^b J_0(t) t^{d_f-1} dt. \quad (12)$$

Since the asymptotic form of the Bessel function  $J_0(t)$  is oscillatory [13]  $J_0(t) \sim \sqrt{(2/\pi t)} \cos(t - \pi/4)$ , the asymptotic form of  $I(b)$  is dominated by  $I_1(b)$  :

$$I_1(b) = \int_0^b t^{d_f-3/2} \cos t dt. \quad (13)$$

Cutting the range of integration into intervals of length  $\pi$  enables us to obtain  $I_1(b)$  as an alternating series with for approximate general term  $u_n$ , when  $n$  is large enough :

$$u_n = n^{d_f-3/2} (-1)^n \quad (14)$$

and

$$I_1(b) \approx \sum_{n=1}^{E(b)} u_n$$

where  $E(b)$  is the integer part of  $b$  ( $b-1 < E(b) \leq b$ ). This series development demonstrates that if  $d_f < 3/2$ ,  $I_1$  converges towards a finite value whatever  $b$  may be increased. Then  $A_u$  depends upon  $\theta$  with a power law  $\theta^{-d_f}$  quite different from that of the first approach. If  $d_f \geq 3/2$ , considering the series  $v_n$  of general term  $v_n = u_{2n} + u_{2n+1}$  demonstrates that  $I_1(b)$  behaves like  $u_{E(b)}$ . Thus, in that case,  $A_u$  is well approximated by  $B_u$  with

$$B_u = d_f \sqrt{2\pi} D \left(\frac{a}{2}\right)^{d_f} (a)^{-3/2} \left(\frac{\lambda}{\pi\theta}\right)^{3/2} \quad (15)$$

Here  $B_u$  depends on  $\theta$  with a power law independent of  $d_f$ , namely  $-3/2$ , and the intensity  $I_u$  decreases as  $\theta^{-3}$ . Thus the two approaches lead to quite different results and, in the radial approach, a threshold  $d_f = 3/2$  defines the transition from an intensity spectrum  $I(\theta)$  with a  $\theta^{-2d_f}$  power law to a  $\theta^{-3}$  power law. And it must be noticed that this same value  $d_f = 3/2$  is an estimate of the percolation threshold in these random Sierpinski carpets [10].

Moreover, as said in the Introduction, the formalism of transfer matrix in fractals gives evidence for correcting terms in the scaling of the structure [11]. In the case of random Sierpinski carpets, the local connectivity defines 6 categories of sites as shown in figure 1 : the isolated square, the square with one neighbour, the square with two neighbours where the three squares define a bar, the square with two neighbours all of them defining a corner, the square with three neighbours and the square with four neighbours. The transfer matrix

$M$  gives the evolution of the statistical average of the number of sites of each category. The recurrent rules of construction of  $C(n, p)$  do not depend upon the step of iteration, what ensures the Markovian character of the process and the interest of the transfer matrix  $M$ . Starting from a physical state  $V$ , which is described by the  $V_i$ 's — the statistical average of the number of square  $i$  —, defines a column vector  $V$  in this 6d space. After a first step of iteration, the vector  $MV$  has for element  $j$  :  $(MV)_j = \sum_i M_{ij} V_i$ , the statistical average of the number of squares  $j$  obtained after one iteration. After  $h$  steps of iteration, similar results are deduced from  $(M^h V)_j$ , which can be easily expressed when diagonalizing the  $M$  matrix.

The  $M$  matrix reads [10, 12] :

$$M = ( T T + P T + 2 P T + 2 P + Q T + 3 P + 2 Q T + 4 P + 4 Q ) \tag{16}$$

where  $T$  is a 6-vector whose coordinates are the mean number of isolated squares and squares with respectively 1, 2 non adjacent, 2 adjacent, 3 and 4 occupied neighboring squares which come from the segmentation of one isolated square. The elements on the six-vector  $P$  are the corrections induced by the existence of a connected edge at the previous step and the elements of the four vector  $Q$  are the corrections induced by the existence of a connected apex between two adjacent connected edges at the previous step. A simple and general calculation gives the eigenvalues of  $M = p, p^2/n^3, (p/n^2)^3$  and 0 thrice degenerate [10] and the calculation of  $M^h$  follows :

$$(M^h)_{i,j} = \alpha_{i,j} p^h + \beta_{i,j} \left( \frac{p^2}{n^3} \right)^h + \gamma_{i,j} \left( \frac{p}{n^2} \right)^{3h} \tag{17}$$

Thus the mean number of squares of category  $i$  obtained after  $h$  steps of iteration from a given configuration is

$$N_i(h) = \sum_{\alpha} a_{i,\alpha} s_{\alpha}^h \tag{18}$$

where  $s_{\alpha}$  means a running non-null eigenvalue of  $M$ , i.e. here,  $p, p^2/n^3$  or  $(p/n^2)^3$ , while the side  $a_h$  of a small square measures

$$a_h = a n^{-h} \tag{19}$$

where  $a$  is the measure of the side of the initial squares.

The area  $s_h$  of a small square is

$$s_h = a^2 n^{-2h} \tag{20}$$

Thus the average density  $\rho_i(h)$  of squares  $i$  after  $h$  steps of iteration is

$$\rho_i(h) = \frac{N_i(h)}{a^2} = \sum_{\alpha} \frac{a_{i,\alpha}}{a^2} \left( \frac{a}{a_h} \right)^{d_{\alpha}} \tag{21}$$

where the subdimension  $d_{\alpha}$  is classically defined [9] as

$$d_{\alpha} = \text{Ln}(s_{\alpha})/\text{Ln}(n) . \tag{22}$$

Such a formula introduces these correction dimensions  $d_{\alpha}$  to the fractal density as introduced in equations (2) and (8) for the two approaches. The meaning of equation (21) can be outlined by a « differential » or « marginal » approach achieved when comparing the

evolution of two systems. Assuming a given starting state  $V$ , an isolated square for instance, there is a finite probability to find a similar state after one step of iteration. The location of this similar state defines what will be called the center of the structure. Then after  $(h + 1)$  steps of iteration from the beginning in the center everything happens as if it were only the  $h$ -th step of iteration, of an isolated square in the previous example. Thus the peripheral density comes from the difference between  $N_i(h + 1)$  and  $N_i(h)$ , and occurs at an average distance  $a$  from the center

$$\rho_{i,h+1}(a) = \sum_{\alpha} \frac{a_{i,\alpha}}{a^2} \left( \frac{a}{a_{h+1}} \right)^{d_{\alpha}} \frac{1 - \left( \frac{a_{h+1}}{a_h} \right)^{d_{\alpha}}}{1 - \left( \frac{a_{h+1}}{a_h} \right)^2} \tag{23}$$

In this formula two singular values of  $d_{\alpha}$  appear :

—  $d_{\alpha} = 2$ , this is the dimension of a plane tiling, and the segmentation ratio  $a_{h+1}/a_h$  plays no part at all, and

—  $d_{\alpha} = 0$ , there is no peripheral density. Moreover, when  $d_{\alpha} < 0$ , the peripheral density becomes negative. This is the sign of a transition towards localization. It must be noted that the existence of a subdimension  $d_{\alpha} = 0$  has been demonstrated to be a criterion of threshold of percolation for a random Sierpinski carpet [10]. This is the same transition between localization and infinite extension which occurs here.

In equations (5) and (10) the diffraction amplitude is directly linked to the surface density  $\rho_s$  and not to the square density  $\rho_i$ , with obviously :

$$\rho_s(r) = \frac{N_i(h) s_h}{s_0} = \rho_i a^2 n^{-2h} = \sum_{\alpha} \frac{a_{i\alpha}}{a^2} \left( \frac{a}{a_h} \right)^{d_{\alpha}-2} \tag{24}$$

Assuming that this local surface density does not depend on the direction  $\theta$  as in the second approach gives

$$\rho_s(r, \theta) = \sum b_{i,\alpha} r^{d_{\alpha}-2} \tag{25}$$

exactly as in equation (9), which proves that the subdimensions  $d_{\alpha}$  generalize the fractal dimension  $d_f$ . The normalized amplitudes  $A_i$  of the diffraction pattern in direction  $\beta$  with wavevector amplitude  $k$  are [1] :

$$A_{i(k)} = \iint \exp[ikr \cos(\theta - \beta)] r dr \frac{d\theta}{2\pi} \rho_s(r, \theta). \tag{26}$$

Using series of Bessel functions of integer order to write the exponent [13] gives :

$$\cos [z \cos(\theta - \beta)] = J_0(z) + 2 \sum_{p=1}^{\infty} (-1)^p J_{2p}(z) \cos [2p(\theta - \beta)] \tag{27}$$

$$\sin [z \cos(\theta - \beta)] = 2 \sum_{p=1}^{\infty} (-1)^p J_{2p+1}(z) \cos [(2p + 1)(\theta - \beta)]. \tag{27 bis}$$

After integration over  $\theta$ , the normalized amplitude is isotropic and reads

$$A_i(k) = \int_0^a \sum_{\alpha} J_0(kr) b_{i,\alpha} r^{d_{\alpha}-1} dr \tag{28}$$

which generalizes equation (11) and when using the series development of Bessel function in powers of its argument [13]:

$$J_0(kr) = \sum_{t=0}^{\infty} \frac{(-1)^t \left(\frac{kr}{2}\right)^{2t}}{(t!)^2} \tag{29}$$

the diffraction amplitude  $A_{i(k)}$  can be broken into several components with :

$$A_i(k) = \sum_{\alpha} A_{i, \alpha(k)} b_{i, \alpha} \tag{30}$$

$$A_{i, \alpha(k)} = \sum_{t=0}^{\infty} (-1)^t \left(\frac{k}{2}\right)^{2t} \frac{1}{(t!)^2} \cdot \frac{1}{2t + d_{\alpha}} [r^{2t + d_{\alpha}}]_0^a. \tag{30 bis}$$

When performing the integration over  $r$ , it has been assumed that  $2t + d_{\alpha}$  is larger than zero ; if not, a cut-off must be introduced for small  $r$  and logarithmic singularities appear when :

$$\begin{aligned} d_{\alpha} &= 0 \\ d_{\alpha} &= -2, \quad d_{\alpha} = -2n. \end{aligned} \tag{31}$$

Such singularities occur for

$$\begin{aligned} d_f &= 2 \left( \left(\frac{p}{n^2}\right)^3 = 1 \right), & d_f &= \frac{3}{2} \left( \frac{p^2}{n^3} = 1 \right), \\ d_f &= \frac{4}{3} \left( \left(\frac{p}{n^2}\right)^3 = \frac{1}{n^2} \right), & d_f &= \frac{2}{3} \left( \left(\frac{p}{n^2}\right)^3 = \frac{1}{n^4} \right) \\ d_f &= \frac{1}{2} \left( \frac{p^2}{n^3} = \frac{1}{n^2} \right) & \text{and} & \quad d_f = 0 \left( \left(\frac{p}{n^2}\right)^3 = 1 \right). \end{aligned}$$

And we meet again the singularity for  $d_f = 3/2$ , here for  $C(4, 8)$ , where, as shown in the convergence argument, the diffraction profile changes. The singularities for  $t = 0$  are uniformly observed in the  $k$  space as shown in equation (30 bis). In other cases the singularities are obtained for  $d_{\alpha} + 2 = 0$  or  $d_{\alpha} + 4 = 0 \dots$  Then decreasing  $d_f$  from 2 the first singularity is obtained when  $d_f = 4/3$ , here  $p = 4^{4/3} = 6.35$ . Thus in the whole observed range from  $p = 9$  to 15 there is no such singularity and the components of the diffraction amplitude take the form :

$$A_{i, \alpha}(k) = f_{i, \alpha}(ka) a^{d_{\alpha}} \tag{32}$$

$$f_{i, \alpha}(x) = \sum_{t=0}^{\infty} (-1)^t \left(\frac{x}{2}\right)^{2t} \frac{1}{(t!)^2} \frac{1}{2t + d_{\alpha}} \tag{32 bis}$$

Equation (32) means that the self similarity of the diffraction pattern is weighted by powers  $d_{\alpha}$  of the size  $a$ . This gives a measurable meaning to  $d_{\alpha}$ . For instance, if the size  $a$  is increased up to  $a'$ , the same diffraction pattern as for  $k$ , will be observed for a reduced wavevector  $k'$  such as  $k' a' = ka$ , but the resulting diffraction amplitude  $A$  will be a sum of  $a^{d_{\alpha}} f_{\alpha}(ka)$  over the different  $d_{\alpha}$  defined from the eigenvalues  $s_{\alpha}$  of the transfer matrix. This analysis for different  $a$  must be done for each spot of the diffraction pattern, and can reveal the spectrum of  $d_{\alpha}$ .

### 3. Experimental results.

Three kinds of diffraction experiments have been done : comparison of diffraction patterns for  $C(4, p)$  with  $p$  varying from 6 to 15, at the fourth step of iteration — comparison of diffraction patterns obtained for different levels of iteration 2, 3 and 4 for  $C(4, 13)$  — and numerical analysis of the intensity ratios along one axis for  $C(4, 13)$  at the steps of iteration 2, 3 and 4. The purposes of these different experiments are to check the dependence of the diffraction pattern upon the fractal dimension, the sensitivity to the level of fractability i.e. to the number of steps of iteration and the evidence for fractal subdimensions and self-similarity.

**3.1 DEPENDENCE UPON FRACTAL DIMENSION.** — Figure 4 shows the diffraction patterns produced by the random Sierpinski carpets with  $p = 6$  (a),  $p = 8$  (b),  $p = 9$  (c),  $p = 10$  (d),  $p = 11$  (e),  $p = 13$  (f),  $p = 14$  (g) and  $p = 15$  (h), where the letter labels the photograph. There are numerous photographs near the theoretical threshold which occurs for  $p = 8$ . There are quite less diffracting pupils for low  $p$  than for high values of  $p$ , what explains the low interest of diffraction patterns for  $p = 5$  and  $p = 7$ . Different features can be noticed. The four external points observed in each pattern correspond to the diffraction of the lattice of small squares which is the framework of these random Sierpinski carpets. Secondly there is a structuration of the pattern inside these 4 points especially for high  $p$ , this structuration corresponds to the existence of blocks of several adjacent squares. Moreover, when  $p$  is rather large, two perpendicular lines appear, as expected for parallel slits [1]; this occurs when percolation is expected to occur, i.e.  $p > 8$ . And on these lines, there are some bright spots regularly spaced. Such spots are expected to be due to the presence of numerous blocks of a few adjacent squares as observed by previous authors [2] for different cluster profiles.

The central part of the diffraction pattern is isotropic and thus deserves the application of the second approach which is linked to the local isotropy of the fractal figures. Thus the profiles are the same for all patterns with  $p \geq 8$  they obey a  $\theta^{-3}$  law as expected from equation (15). The only difference in this central part comes from the intensity of the diffraction patterns since the diffracting area is proportional to  $p^4$  for this 4th step of iteration, and thus to  $e^{4d_f}$ .

**3.2 INFLUENCE OF THE NUMBER OF STEPS OF ITERATION.** — In figure 5 we plot the diffraction patterns of  $(4, 13)$  at the steps of iteration : 2 (Fig. 5a), 3 (Fig. 5b) and 4 (Fig. 5c). Of course the 0 step of iteration is a full square which gives rise to a cross for diffraction pattern as is well known [1, 2]. The transition from a bi-axial symmetry, with this cross as a distinctive feature, as is obvious in figure 5a, to a nearly isotropic symmetry with a full disc as diffraction pattern, as is obvious in figure 5c, is well observed in figure 5b. The appearance of numerous points in the diffraction pattern is linked to the appearance of periodicity or nearly periodicity in the pupil and increases when the order of the step of iteration is increased, and more distant points appear, revealing shorter periodicities as obvious in the framework. Besides these points, larger and larger nearly continuous bright areas appear in the diffraction pattern as expected from fractal figures with a high level of randomness.

**3.3 NUMERICAL ANALYSIS OF THE DIFFRACTION PATTERN.** — Along the axis  $Ox$  the slit of a photomultiplier detector is put and is moved with a uniform speed which enables to obtain numerically the diffracted intensity  $I$  as a function of  $\theta$ . The experiments have been done for typical Sierpinski carpets  $C(4, p)$  with  $p = 11, 12, 13$  and  $14$ , at different levels of iteration. Firstly, the central profiles i.e. the continuous part of diffraction patterns at the fourth step of iteration have been observed for  $C(4, p)$  with  $p = 11, 12, 13$  and  $14$  as shown in figure 6. The

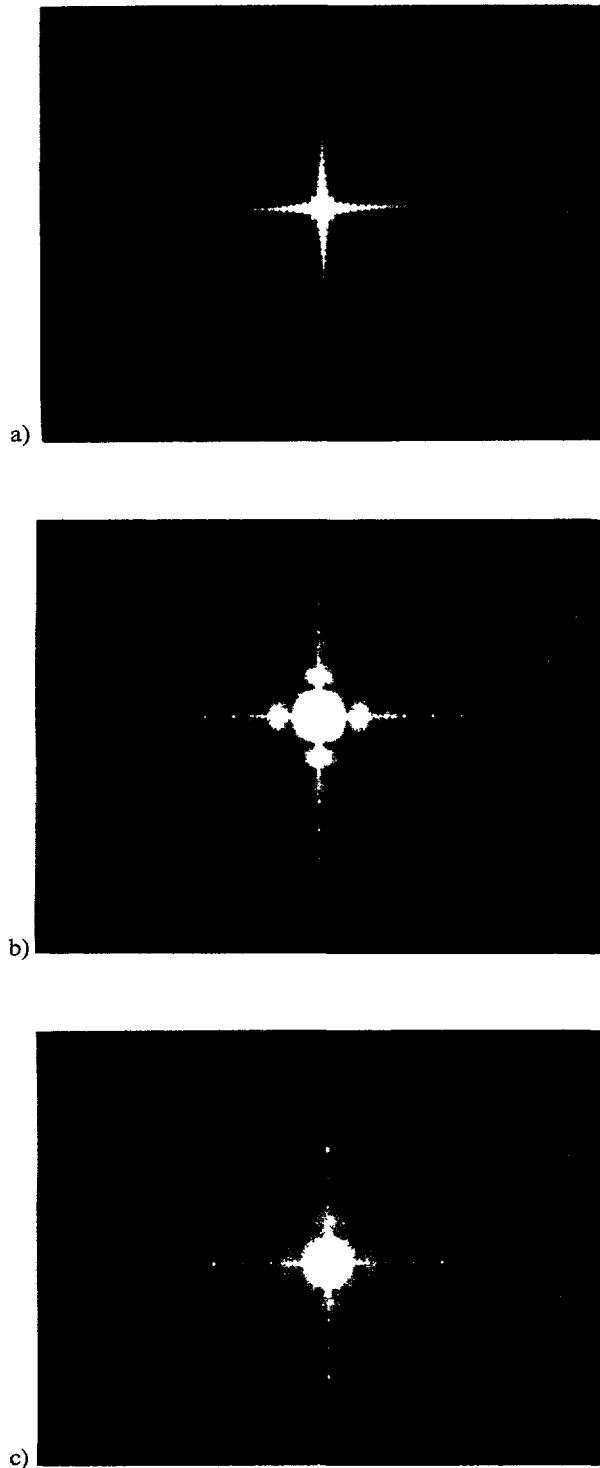


Fig. 5. — Diffraction patterns obtained from C (4, 13) at different levels  $k$  of iteration. a)  $k = 2$ , b)  $k = 3$  and c)  $k = 4$ . The transition from the cross which is the diffraction pattern of a square to a nearly continuous profile as expected for fractal is quite obvious.

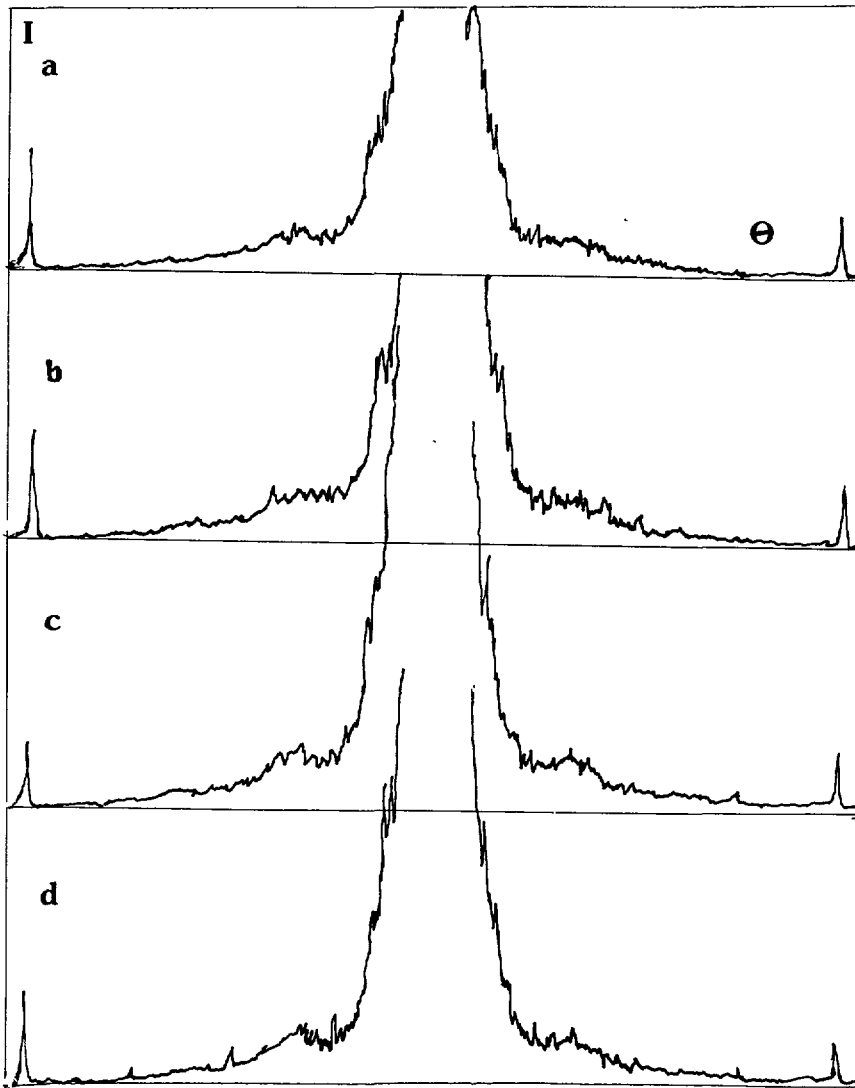


Fig. 6. — The central profiles of diffraction patterns at the fourth step of iteration for  $C(4, p)$  with a)  $p = 11$ , b)  $p = 12$ , c)  $p = 13$ , d)  $p = 14$ .

intensity  $I_{(\theta)}$  decreases from the center of the line with a quite similar power law where the exponent is nearly  $3(\pm 0.5)$  in all cases. But the fluctuations are quite important. Since the basis formula (15) is well verified and fluctuations are rather strong, the observation of correction scaling dimensions seems to be out of scope. More exactly, it is interesting to directly analyze the distribution of connectivity for different samplings  $C(n, p)$  and to compute the amplitude of statistical fluctuations. The results are shown in table I for  $C(4, 12)$  at the fourth step of iteration for a statistics of 14 different trials.

From these results it appears that the observation of correction scaling dimensions requires a high level of statistics in order to reduce the relative size of statistic fluctuations to be lower than the correction of the scaling law. Here this is not realized, since for a rather low step of iteration 2 for instance the statistics are poor, there are only a small number of sites and for a

Table I. — Percentages of squares which are isolated  $t_i$ , with one neighbour  $t_1$ , with two opposite neighbours  $t_{d2}$ , with two non-opposite neighbours  $t_{c2}$  with three neighbours  $t_3$  and with four neighbours. On the second line, the standard deviation  $\delta t$  is given.

	$t_i$	$t_1$	$t_{d2}$	$t_{c2}$	$t_3$	$t_4$
$t$	0.0077	0.0756	0.0920	0.2027	0.4268	0.1950
$\delta t$	0.0009	0.0027	0.0016	0.0031	0.0034	0.0022

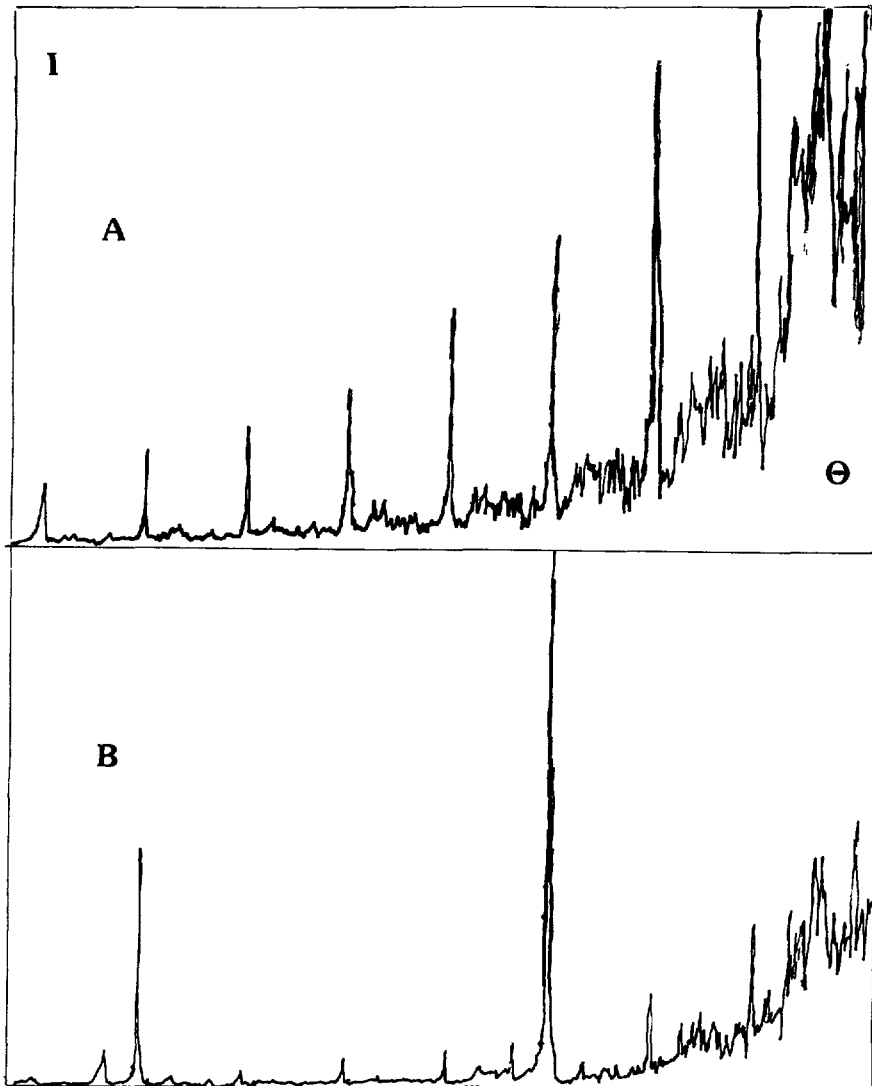


Fig. 7. — The profiles for diffraction points for  $C(4, 13)$  at  $k = 3$  in a) and  $k = 4$  in b).

large step of iteration  $k > 4$ , the weight of correction scaling dimensions is weak in front of that of the main fractal dimension. Thus numerical diffraction with a high level of statistics is recommended to check these parameters.

The self similarity of diffraction patterns is well observed at different levels of iteration and instead of directly determining the correction scaling dimensions, it is of interest to compare the profiles for diffraction points observed for  $C(4, 13)$  at  $k = 3$  and 4 as shown in figure 7. It must be noticed that both profiles follow a power law  $I_{(n)} = n^{-d}$ , with as exponent  $d$ , 1.3 for  $k = 3$  and 1.5 for  $k = 4$ . From equations (32) which generalize equations (11) and (15) the expected exponent is  $2d_f = 3.7$  or 3 while the other exponents of the series are  $3d_f - 3 = 2.55$ ,  $4d_f - 6 = 1.4$ ,  $5d_f - 9 = 0.25$ ,  $6d_f - 12 = -0.9$ . Moreover the large real exponent  $2d_f$  is only expected for a large number of steps of iteration, which is in agreement with the increase of  $d$  with  $k$ . Thus this result confirms the role of correction scaling terms, which can be fitted.

Finally, even if the correction scaling exponents are not found precisely, there are numerous proofs of their existence and it is clearly suggested that when improving the statistics by means of computing the diffraction pattern an accurate measurement of these exponents can be achieved. And the threshold  $d_f = 3/2$  is well estimated to define a transition in diffraction patterns.

#### References

- [1] HECHT E., Optics (Addison Wesley editors, 2nd Edition, Reading, Mass., 1987).
- [2] KAYE B. H., A random walk through fractal dimensions, V. C. H. Verlag, Berlin (1989), quoting the M. Sc ; thesis of LEBLANC J. (1986) and MURPHY R. (1972) both at Laurentian University.
- [3] MACKAY A. L., *Physica* **114A** (1982) 609.
- [4] WARRINGTON D. H., in Quasicrystalline Materials, C. Janot and J. M. Dubois Eds. (World Scientific, Singapore, 1988) p 243.
- [5] PERREAU M., COSTE J. P., BERGER D., MERCIER D. and LEVY J. C. S., Basis Features of their Glassy State, J. Colmenero and J. Alegria Eds. (World Scientific, Singapore, 1990) p. 73.
- [6] SCHECHTMAN D., BLECH I., GRATIAS D. and CAHN J. W., *Phys. Rev. Lett.* **53** (1984) 1951.
- [7] BENDERSKY L., *Phys. Rev. Lett.* **55** (1985) 1461.
- [8] ALLAIN C. and CLOITRE M., *Physica A* **157** (1989) 352.
- [9] MANDELBROT B. B., The fractal geometry of nature (Freeman ed., New York, 1983).
- [10] PERREAU M. and LEVY J. C. S., *Phys. Rev. A* **40** (1989) 4690.
- [11] MANDELBROT B. B., GEFEN Y., AHARONY A. and PEYRIERE J., *J. Phys. A* **18** (1985) 335.
- [12] PERREAU M., Thesis Paris 1990, Université Paris 7, unpublished.
- [13] ABRAMOWITZ M. and STEGUN I., Handbook of Mathematical functions, National Bureau of Standards (1964) Washington D.C.